Characteristics of a wake-vortex tracking system based on acoustic refractive scattering

David C. Burnham

U. S. Department of Transportation, Transportation Systems Center, Kendall Square, Cambridge, Massachusetts 02142

(Received 20 July 1976; revised 21 November 1976)

The theory of acoustic-ray bending by aircraft-generated vortices is developed in a form convenient for application to a practical vortex tracking system. The maximum scattering angle θ_m is proportional to the vortex circulation divided by the average core radius. Since the circulation for commercial jet transports is roughly proportional to the wingspan, the value of θ_m depends little on aircraft size but strongly on the ratio of the core size to the wingspan. For landing aircraft θ_m varies from 0.5 to 1.4 rad depending upon the engine placement. A variety of vortex core models are considered which lead to values of θ_m between 0.2 and 0.9 rad. The capabilities of a pulsed acoustic vortex tracking system depend strongly upon θ_m and therefore upon aircraft type. The effects of timing errors, both vortex induced and random, on tracking accuracy are derived. The fundamental differences between refractive scattering and turbulence scattering techniques are described.

PACS numbers: 43.28. Py, 43.20. Dk, 43.20. Fm.

INTRODUCTION

The possibility of detecting aircraft-generated vortices by means of refractive scattering was discussed by Georges,[1] who calculated acoustic rays for a vortex with a viscous core. The experimental observation of this effect and its use for tracking vortices was reported by Burnham *et al.*[2] in a letter to the Editor. In this paper, the theoretical basis for the observations is discussed, and estimates are made of the accuracy with which vortices can be located. In addition, the properties of a tracking system based on refractive scattering are compared to those of a system employing incoherent acoustic scattering from turbulence imbeded in the vortex.

I. THEORY OF RAY BENDING

The geometrical ray approximation describes the propagation of sound when the variations in wind velocity $\mathbf{v}$, sound speed c (which depends upon temperature but not pressure), and acoustic impedance are small over distances of one wavelength λ. Sound travels along a ray which is defined by $\mathbf{r}(s)$, the position of the ray as a function of the distance s along the ray. Deviations from this picture of acoustic propagation are caused by diffraction and incoherent scattering from fluctuations and inhomogeneities.

Considerable work[1,3,4] has already been done on the problem of computing the exact geometrical propagation of sound through several model vortices. We adopt a somewhat different approach, which views the propagation as a scattering process. Some simple analytical results are obtained from the impact approximation which assumes that the ray passes through the vortex on a straight line. When terms in v/c higher than first order are neglected, the vector ray equation takes the simple form[5]

$$\frac{d\mathbf{n}}{ds} + \mathbf{n}\times(\nabla\times\mathbf{v}/c) = 0 , \tag{1}$$

where c and the fluid density ρ are assumed constant, and $\mathbf{n} = d\mathbf{r}/ds$ is the unit vector tangent to the ray. The effects of the vortex velocity are much stronger than those of the reduced density and possible increased temperature in the vortex core, which are neglected in this approximation. Since the maximum observed velocities in aircraft vortices are less than $v/c = 0.2$, higher-order terms in v/c can also be neglected.[6] The effect of Eq. (1) is to rotate the direction of the ray about an axis parallel to the curl of the velocity field, $\gamma = \nabla\times\mathbf{v}$, where γ is called the vorticity of the field.

For a cylindrically symmetric vortex the vorticity $\gamma(r)$ is a function of the radius r from the vortex axis. The other properties of the vortex can be expressed as integrals of $\gamma(r)$. The circulation is

$$\Gamma(r) = 2\pi \int_0^r \gamma(r')\, r'\, dr' , \tag{2}$$

and the tangential velocity is

$$v(r) = \Gamma(r)/2\pi r . \tag{3}$$

An aircraft wake vortex is normally represented by a central-core region where the vorticity γ is large and an outer region where γ is small or zero. In this case, the circulation for infinite radius $\Gamma(\infty)$ has a well-defined value and the velocity in the outer region is approximately that of a line vortex of strength $\Gamma(\infty)$. The size of the vortex core is normally characterized by the radius a where the velocity reaches a maximum.

Table I mathematically defines the three models which we will use to represent wake vortices. Georges[1] used a fourth model, the viscous core. These three models were used to generate the four velocity profiles shown in Fig. 1, which will be used in subsequent calculations. The model parameters are listed in Table II and discussed below. The parameters selected are appropriate for a wake vortex from a Boeing 747 aircraft with a wing span b of 60 m. All four velocity profiles have a vortex strength of 500 m^2/sec. In the solid-core model, the velocity is proportional to r up to radius a and then decreases inversely with r. Spreiter

TABLE I. Votex core models.[a]

	Model definition				Impact-approximation results		
Model	Range	$\Gamma(r)$	$2\pi\gamma(r)$	$\bar{r}$	Range	$c\theta(p)$	$c[c\tau(p)+2p\theta(p)]$
Solid core	$r>a$	$\Gamma(\infty)$	0	$\frac{1}{2}a$	$p>a$	0	$\Gamma(\infty)p/2\lvert p\rvert$
	$r<a$	$\Gamma(\infty)(r/a)^2$	$2\Gamma(\infty)a^2$		$p<a$	$2\Gamma(\infty)[1-(p/a)^2]/a\pi$	$\frac{\Gamma(\infty)p(2\phi_a+\sin 2\phi_a)}{2\pi\lvert p\rvert}$
logarithmic core	$r>r_m$	$\Gamma(\infty)$	0		$p>r_m$	0	$\Gamma(\infty)p/2\lvert p\rvert$
	$a^*<r<r_m$	$\Gamma(a)[\ln(r/a)+1]$	$\Gamma(a)/r^2$	$\frac{\frac{1}{2}a^*\Gamma(\infty)}{(1-a^*/2r_m)\Gamma(a)}$	$a^*<p<r_m$	$\Gamma(a)\phi_m/\lvert p\rvert\pi$	
	$r<a^*$	$\frac{1}{2}\Gamma(a)(r/a^*)^2$	$\Gamma(a)/a^{*2}$		$p<a^*$		
Simple		$\frac{\Gamma(\infty)r^2}{r^2+a^2}$	$\frac{2\Gamma(\infty)a^2}{(r^2+a^2)^2}$	$2a/\pi$		$\frac{\Gamma(\infty)a^2}{2(p^2+a^2)^{3/2}}$	$\frac{\Gamma(\infty)p}{2(a^2+p^2)^{1/2}}$

[a]Definitions of new symbols: $a^*\equiv a/e^{1/2}$; $r_m\equiv a\exp[\Gamma(\infty)/\Gamma(a)-1]$; $\sin\phi_a\equiv\lvert p\rvert/a$; $\cos\phi_m\equiv\lvert p\rvert/r_m$.

and Sacks[7] estimate a core radius $a=b/12.9$ for this model. The log-core model was proposed by Hoffman and Joubert[8] to describe a turbulent vortex. The values $\Gamma(a)/\Gamma(\infty)=0.16$ and $a=0.30$ m were proposed by McCormick *et al.*[9] This model requires some modification at small and large radii to avoid divergences. We make a transition to a solid core at the radius $a/e^{1/2}$ which gives continuous vorticity, and eliminate vorticity beyond the radius where $\Gamma(r)=\Gamma(\infty)$. The third vortex model is a simple form we have used to fit vortex-velocity data obtained from an acoustic backscatter system.[10] This model has the simple feature that $\Gamma(a)=\frac{1}{2}\Gamma(\infty)$. Two values of core radius are selected for the simple model since the core radius is adjustable for this model.

The geometry of the ray calculation is shown in Fig. 2. We take γ in the z direction and express r in cylindrical (r, ϕ) or Cartesian (x, y) coordinates concentric with the vortex core. We assume that the acoustic ray is incident along the x axis at an impact parameter $y=p$. According to Eq. (1), the acoustic ray is deflected only when the vorticity is nonzero.[6] One can integrate Eq. (1) through the vortex core to find the total angle $\theta(p)$ through which the ray is bent. The details of this calculation appear in the Appendix. Values of this scattering angle $\theta(p)$ are plotted in Fig. 3(a) for the four cases of Table II. The maximum scattering angle occurs for a negative impact parameter because the ray must start off somewhat below the x axis in Fig. 2 in order to pass through the center of the vortex where $\gamma(r)$ is greatest.

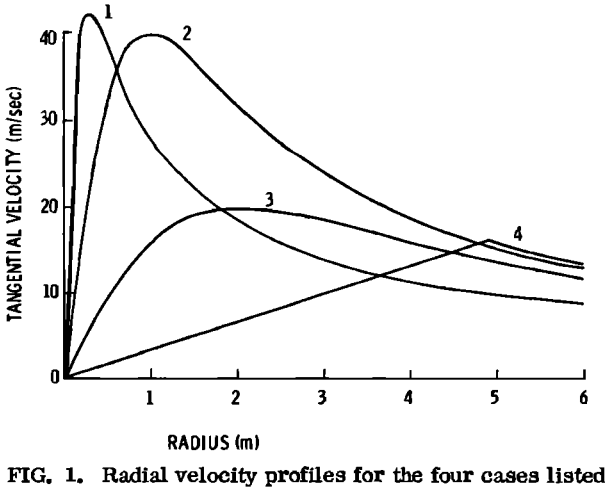

FIG. 1. Radial velocity profiles for the four cases listed in Table II.

The existence of a maximum scattering angle θ_m in Fig. 3(a) has important implications for a vortex tracking system based on acoustic-ray bending. Such a system will be discussed in Sec. III. A useful estimate (see Table II for a comparison) for the value of θ_m can be determined from the impact approximation discussed in the Appendix,

$$c\theta_m=2\int_0^\infty\gamma(r)\,dr=\Gamma(\infty)/\pi\bar{r}\,. \tag{4}$$

We have defined an "average core radius" $\bar{r}$ by

$$\bar{r}=\int_0^\infty r\gamma(r)\,dr\Big/\int_0^\infty\gamma(r)\,dr \tag{5}$$

in order to relate θ_m to the strength $\Gamma(\infty)$. For a particular model of the vortex core one can express θ_m in the simpler form $\theta_m=Kv_m/c$ (see Georges[1]) where v_m is the maximum tangential wind speed and K is a number of order unity which depends upon the core model. Since $\Gamma(\infty)$ is defined by aircraft parameters [see Eq. (10)], Eq. (4) has the advantage of collecting the core-dependent characteristics of the vortex, which are generally unknown, into one parameter $\bar{r}$ rather than two (K, v_m).

Since the tracking system in Sec. III locates the vortex by means of the acoustic propagation time, it is desirable to investigate the propagation-time change $\tau(p)$ introduced by the vortex itself. The appropriate reference time for this purpose is the propagation time for scattering from a point scatterer located at the same

TABLE II. B-747 vortex parameters, $\Gamma(\infty)=500$ m^2/sec, $b=60$ m.

Case	Model	$a(m)$	θ_m(rad)	θ_m(impact)
1	$\log[\Gamma(a)/\Gamma(\infty)]=0.16$	0.3	0.85	0.84
2	simple	1.0	0.76	0.75
3	simple	2.0	0.38	0.37
4	solid	4.9	0.20	0.19

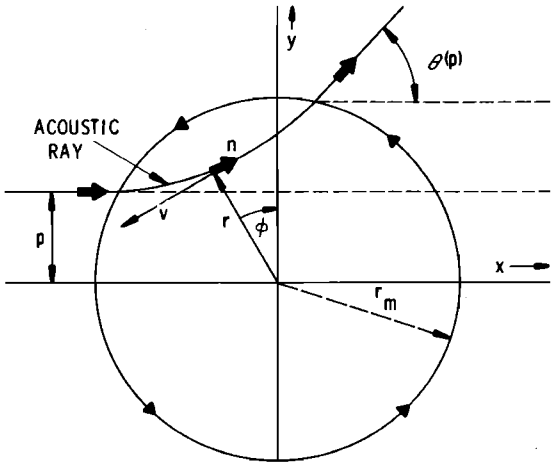

FIG. 2. Scattering geometry. The circle encloses the region of nonzero vorticity.

position as the vortex center. To first order in v/c the effective sound speed along a ray is[5] $c+\mathbf{n}\cdot\mathbf{v}$. The time error for $v \ll c$ becomes

$$c\tau(p) = \int ds(1-\mathbf{n}\cdot\mathbf{v}/c) - \int_c ds \tag{6}$$

where the first term is evaluated along the actual ray path and the second along straight lines meeting at the vortex center. The details of this calculation appear in the Appendix. When the impact parameter is far outside the core ($|p| \gg a$) the path of integration in Eq. (6) is a straight line and the integral can be evaluated to give

$$\tau(\infty) = \pm\Gamma(\infty)/2c^2\,, \tag{7}$$

where the sign depends upon which side of the core the path passes. Computed values of $\tau(p)$ for the four cases in Table II are plotted in Fig. 3(b). The values of $|\tau|$ are generally much less than the limiting value $|\tau(\infty)|$ from Eq. (7) because the two terms contributing to Eq. (6) have opposite signs. The change in path length $[\int ds - \int_c ds]$ tends to cancel the effect of the vortex wind $[-\int ds\,\mathbf{n}\cdot\mathbf{v}/c]$.

The impact parameter p cannot be measured experimentally. Only scattering angles, time delays, and cross sections are observable. Figure 4 shows the results of Fig. 3 replotted as time error versus scat-

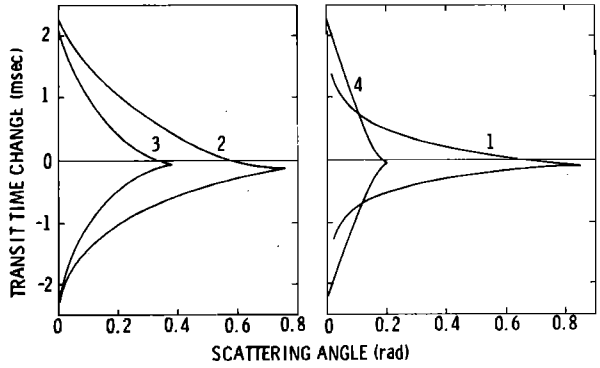

FIG. 4. Transit time change versus scattering angle for the data of Fig. 3.

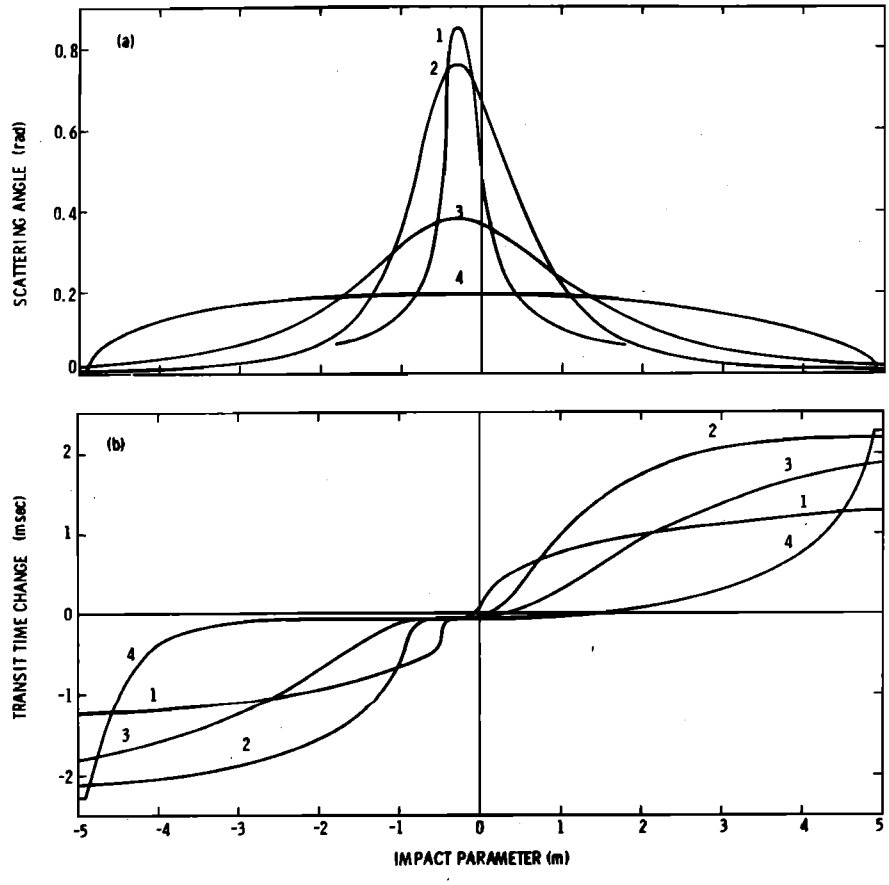

FIG. 3. Scattering angle (a) and transit time change (b) versus impact parameter for the four gases in Table II.

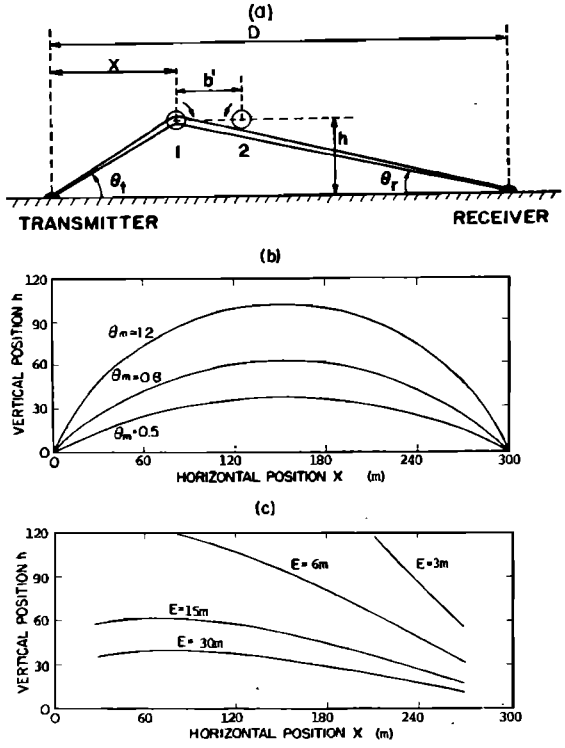

FIG. 5. Experimental geometry of a pulsed acoustic system for locating aircraft vortices in a plane perpendicular to the aircraft path. $D_1 = 300$ m. (a) Locations of transmitter, receiver, and vortex pair, (b) contours of constant maximum scattering angle (θ_m in rads), (c) contours of constant error E for a two receiver system ($D_2 = 1.4\ D_1$) in which the time delay for the second receiver is in error by -2 msec.

tering angle. For a given scattering angle two propagation times occur, corresponding to rays passing on either side of the vortex center. For zero scattering angle this splitting ΔT approaches $\Gamma(\infty)/c^2$. The average propagation time change remains close to zero. If ΔT is shorter than the duration of the acoustic pulse being scattered, the two scattered signals will interfer since they are coherent. The one-dimensional scattering cross section $d\sigma/d\theta$ is given by

$$\frac{d\sigma}{d\theta} = \left(\frac{d\theta}{dp}\right)^{-1} . \tag{8}$$

An inspection of Fig. 3 for the physically realistic cases 1–3 shows that, apart from the caustic at θ_m, the cross section generally decreases as θ increases. Moreover, a comparison of the slopes of the two branches of the $\theta(p)$ curve indicates that the pulse arriving first should have a smaller amplitude than the one arriving second.

The validity of the ray calculation presented here is limited by incoherent scattering and diffraction, both of which tend to smear out the ray. Although the amount of incoherent scattering is difficult to predict *a priori*, the effect of diffraction can be estimated in a straightforward fashion. The bundle of rays with impact parameter range Δp will be diffracted into a spread in angle $\Delta\theta = \lambda/\Delta p$. The size of Δp is limited by the fact that θ depends upon p: $\Delta\theta = (d\theta/dp)\Delta p$. These two relations can be combined to give a self-consistent value for the spread in scattering angle

$$\Delta\theta = \left[\left(\frac{d\theta}{dp}\right)\lambda\right]^{1/2} . \tag{9}$$

Decreasing the wavelength leads to less smear. The condition for the validity of our calculation is $\Delta\theta \ll \theta$.

II. PROPERTIES OF AIRCRAFT GENERATED VORTICES

This section summarizes the theoretical and experimental properties of aircraft vortices which are relevant to the tracking system discussed in Sec. III. The theoretical results are based on the literature and on Sec. I. The experimental results are based on measurements[2] using a scattering system of the type discussed in Sec. IV [see Fig. 5(a)].

An aircraft traveling at speed V generates a pair of counter-rotating vortices with strength

$$\Gamma(\infty) = 4W/\pi\rho V b \tag{10}$$

(assuming elliptic wing loading), where W is the aircraft weight, b is the wing span, and ρ is the air density. The B-747 strength of 500 m^2/sec used in Table II is based on the parameters $W = 2.5\times10^6$ N (maximum landing weight), $\rho = 1.2$ kg/m^3, $V = 90$ m/sec (landing), and $b = 60$ m. The vortex spacing b' is $\frac{1}{4}\pi b$ for elliptic wing loading. The vortex motion in an atmosphere with uniform horizontal winds can be predicted using simple potential flow theory.[11] After generation the vortices drift downward at speed $w = \Gamma(\infty)/2\pi b'$. As the vortex pair approaches the ground the two vortices separate and travel apart at relative speed $2w$ and at height $\frac{1}{2}b'$.

The B-747 results in Sec. I can be scaled to smaller aircraft by using Eqs. (4) and (10). An important factor in scaling is the consistency of the ratio W/b^2 (the wing loading) for jet transports with high aspect-ratio wings. The values of W/b^2 range from 65% to 100% of the B-747 value even though b varies more than a factor of 2. Another factor in scaling is the ratio k of the wing span to the average core radius $k = b/\bar{r}$. This ratio is a function of the vortex model. For example, the Spreiter and Sacks[7] model yields $k = 26$. According to Eqs. (4) and (10) the aircraft parameter dependence of the maximum scattering angle θ_m is given by $k(W/b^2)/V$. Since the wing loading and landing speed vary little with aircraft type, the observed strong dependence in θ_m for landing aircraft (0.5–1.4 rad) must reflect variations in k. These variations are related to differing flap and engine locations.[12] The vortex models in Sec. I which have specified core sizes (log and solid) also show a strong variation in k, namely, a factor of 4. Although the size of the aircraft has relatively little effect on the predicted maximum scattering angle, it directly affects the propagation-time changes which are proportional to $\Gamma(\infty)$ [Eq. (7)]. The maximum deviation for a single B-747 vortex is approximately 2 msec. Smaller aircraft produce proportionately smaller time errors.

The ray-bending model (Sec. I) for acoustic scattering from aircraft vortices predicts the following features, which are arranged in order of descending certainty:

(1) Acoustic energy is scattered only in the direction of vortex rotation,

(2) the scattered sound is spread out in time by at most $2\tau(\infty)$,

(3) the scattered acoustic signal is split into two pulses whose separation and relative amplitude depend upon the core model.

Prediction (1) has been thoroughly verified. Only one of the two vortices is ever observed by a single acoustic beam [see Fig. 5(a)]. The expected time delay for the other vortex is determined by simultaneously transmitting in the opposite direction using the same pair of transducers. Prediction (2) has been verified for vortices at relatively large scattering angles, as in Fig. 6 for a B-747 aircraft. If the scattering were taking place incoherently across a core of diameter d, one would expect a time spread of $(2d/c)\sin(\frac{1}{2}\theta) \approx d\theta/c$. For a B-747 core with $d = 5$ m and $\theta = 1$ one might expect a time spread of 15 msec. In fact, the spread observed in Fig. 6 is probably less than 1 or 2 msec. However, significant spreading and time fluctuations have been observed for small-angle scattering, particularly under high-wind conditions and for vortices with large cores (i.e., small maximum scattering angles). These effects are probably due to turbulence. On some occasions two distinct scattering signals are observed. The extra signal, probably produced by a vortex from the aircraft elevator, persists for a time of 10 or 15 sec and descends toward the ground at about three times the rate of the main vortex. Prediction 3 has never been observed, even under the most likely conditions of small scattering angles from the largest aircraft (B-747, C-5A). The splitting may be obscured by the direct signal propagating along the ground for the smallest scattering angles observed.

More quantitative predictions of the ray-bending properties of aircraft vortices are best based on the results for the log core or simple model rather than those for the solid-core model which are dominated by the singularity at $p = a$. The impact approximation for the log core gives particularly simple analytical forms,

$$\theta(p) = \delta/|p|\,, \tag{11a}$$

$$\frac{d\sigma}{d\theta} = \frac{2\delta}{\theta^2} \tag{11b}$$

[$\delta \approx \Gamma(a)/2c$ from Table I], which are useful for $\theta < 1$. In Eq. (11b), the scattering cross section includes both branches (Fig. 4) of the scattering curve and neglects any interference between them. The fractional spread in scattering angle caused by diffraction becomes $\Delta\theta/\theta = (\lambda/\delta)^{1/2}$ according to Eqs. (9) and (11a). For the B-747 vortex model in Table II, δ is 0.12 m and $\Delta\theta/\theta$ is approximately unity at 3-kHz acoustic frequency. Since the experimental tests have been performed with frequencies of 2–3 kHz, the ray approximation is at best marginally suitable for B-747 vortices with log cores and is probably unsuitable for log-core vortices from smaller aircraft. The effect of diffraction is to destroy the functional dependence of θ and τ upon p, and, therefore, it may be responsible for the failure of prediction 3 above. Arbitrarily higher frequencies cannot be used to reduce diffraction since the optimum frequency is determined as a compromise between the advantages of low frequency: high transducer efficiency and low atmospheric attenuation,[13] and those of high frequency: greater antenna gain and lower ambient noise.

III. TRACKING SYSTEM

The simplest experimental arrangement we have used for scattering acoustic energy from vortices is shown in Fig. 5(a). The transmitter and receiver are situated at ground level on a base line (length D) perpendicular to the path of the aircraft. Both transmitter and receiver generate vertical fan beams. For a single direction of sound propagation only the vortex closer to the transmitter is rotating in the correct direction to scatter energy into the receiver. Propagation in both directions is required to observe both vortices.

The locations of the transmitter, receiver, and vortex determine the scattering angle θ,

$$\theta = \theta_t + \theta_r\,, \tag{12}$$

where θ_t and θ_r are the elevation angles as seen from the transmitter and receiver, respectively. A scattered signal is observed as long as the scattering angle θ is less than the maximum scattering angle θ_m. Figure 5(b) shows the sensitive volume for vortex detection for several values of θ_m.

For the experimental arrangement shown in Fig. 5(a) theory predicts (Sec. I) three transit times T_i for propagation between the transmitter and the receiver. The shortest is just the time for sound to propagate along the ground,

$$cT_1 = D. \tag{13}$$

The two times associated with scattering from the vortex are ($i = 2$, 3)

$$cT_i = (x^2 + h^2)^{1/2} + [(D-x)^2 + h^2]^{1/2} + \tau_i(\theta)\,, \tag{14}$$

where the τ_i are the two transit times (Fig. 4) relative to the vortex center. Since two scattered signals are never observed experimentally, we will neglect τ_i for the present discussion. A measured value of T_2 ($\equiv T_3$) locates the vortex on an ellipse with foci at the transmitter and receiver. When the scattering angle θ is small, the ellipse is almost horizontal over the central range of x. There the time delay $T_2 - T_1$ is determined predominantly by the height h. In particular, the height h is given to 12% accuracy by the expression

$$h = [\tfrac{1}{2}c(T_2 - T_1)D]^{1/2} \tag{15}$$

over the range $\frac{1}{4}D < x < \frac{3}{4}D$.

The vortex location can be completely determined if the time delay associated with a different base line (and therefore a different ellipse) is known. For example,

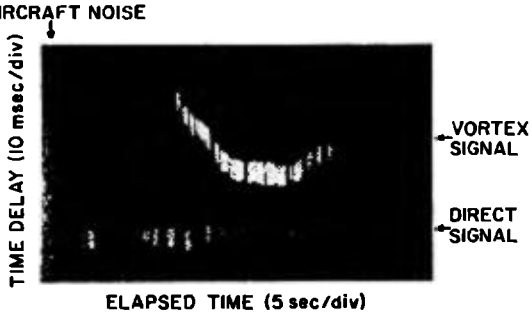

FIG. 6. Acoustic scattering data for a B-747 vortex. Acoustic intensity appears as z-axis intensity on a CRT. The elapsed time begins at the left edge of the picture when the aircraft passes the system baseline ($D=138$ m). The acoustic pulse length is 5 msec.

a second receiver at distance $D_2>D_1=D$ could be added to the system shown in Fig. 5(a). If the first receiver receives a scattered signal for the vortex ($\theta_1<\theta_m$), then the second receiver will also see a scattered signal since $\theta_2<\theta_1$ for $D_2>D_1$. The curves in Fig. 5(b) thus also indicate the sensitive volume for a two-receiver system.

Measuring the time delays for two base lines determines the location of the vortex by the intersection of the two ellipses. For some vortex locations this intersection occurs where the ellipses are almost tangent, and a small error in time can produce a large error in location. For one choice of D_1 and D_2, Fig. 5(c) shows contours of constant error E produced by a fixed error of 2 msec in the time delay associated with the longer base line D_2. The same size error in time delay for the shorter base line D_1 produces less error in position. The position error is defined as

$$E=[(x'-x)^2+(h'-h)^2]^{1/2},$$

where $(x,\ h)$ is the real location and $(x',\ h')$ is the apparent location. As one might expect from the earlier discussion, the errors shown in Fig. 6(c) are predominantly horizontal. The location errors can become extremely large as h decreases, since the time delays generally decrease as h^2 [Eq. (15)]. The resolution improves as the vortex approaches the first receiver because the two ellipses intersect at a greater angle.

The properties of the vortices themselves can introduce systematic errors into the measurement of time delays. These errors are all proportional to the vortex strength $\Gamma(\infty)$ and are therefore larger for larger aircraft. The first potential source of error is the splitting (or perhaps smearing) of the scattered signal shown in Fig. 4 and included in Eq. (14). As θ approaches zero this error could approach a maximum value of $\tau(\infty)$ [Eq. (7)].

A second potential source of error is the effect of the vortices on the direct signal, which corresponds to zero angle scattering. The direct signal is not only affected by a vortex directly but also by its image (position $x,\ -h$), which serves to satisfy the boundary condition of no vertical wind at the surface. Under the conditions $h\ll x,\ h\ll D-x$ the effect of a single vortex on the direct arrival time T_1 is $2\tau(\infty)$. The effect of both vortices and their images can be integrated without the above restrictions to give

$$\Delta T_1=2\tau(\infty)(\theta_2-\theta_1)/\pi\ , \tag{16}$$

where θ_1 and θ_2 are the scattering angles $\theta_t+\theta_r$ for each vortex, respectively, in Fig. 5(a). Direct signal shifts of this sign and magnitude have been observed experimentally. These shifts are larger than those for the scattered signal and are normally eliminated from the time-delay measurement by measuring the average direct arrival time before the aircraft arrival.

A third source of error is due to the influence of one vortex and both image vortices on the scattered signal from the other vortex. These effects can be evaluated in the same way that Eq. (16) was derived, but the resultant expression is much more complicated. Because of cancellations the maximum effect is approximately only $\tau(\infty)$ for realistic scattering angles. One should also note that, if the two vortices are not at equal heights, the scattered signal from one may pass through the core of the other and be deflected away from the receiver. Some indications of such double scattering have appeared in experimental data.

Atmospheric effects on the accuracy of time-delay measurements are not as easily estimated as those due to the vortices themselves. Under ideal conditions random errors in vortex arrival time are probably less than 1 msec (see Fig. 6). Systematic errors in the time delay can be produced by vertical gradients in temperature and wind, since the direct and vortex signals then experience different propagation conditions. For reasonably large scattering angles the effects of beam bending are less important than the direct change in the effective speed of sound. For the low altitudes involved with vortex sensing, wind shear is more significant than the temperature gradient except when a strong ground-based inversion is present. In order to estimate the magnitude of wind-shear effects, let us assume a linear variation with altitude for the wind component along the base line. A wind difference of 1 m/sec between the direct signal altitude and the vortex altitude would give a time error of 1.3 msec for the 300-m base line of Fig. 5. Time variations in the wind can also produce errors if a fixed average direct arrival time is used.

In most of our vortex tracking installations more than two base lines are available for tracking a vortex. Systematic errors regularly show up as consistent discrepancies in vortex location for different combinations of base lines. The relative importance of vortex and atmospheric contributions to these effects has not been determined.

One can estimate the expected relative strength of the direct and vortex signals. If the sound intensity produced by the transmitter in Fig. 6(a) is independent of θ_t, then the ratio of the scattered-signal intensity to the direct-signal intensity can be evaluated, neglecting attenuation

$$\frac{I_s}{I_D} = \frac{D\, d\sigma/d\theta}{(x^2+h^2)[(D-x)^2+h^2]^{1/2}} \times \frac{D}{(x^2+h^2)^{1/2}+[(D-x)^2+h^2]^{1/2}} \quad . \tag{17}$$

The first factor is due to the one-dimensional scattering in the vertical plane. The second is the result of the extra propagation distance on the beam spreading in the transverse dimension. Equations (17) and (11b) can be combined to yield an approximate result for a vortex located roughly midway between the transmitter and receiver

$$I_s/I_D \approx 8\delta/D\theta^2 \ . \tag{18}$$

These calculated acoustic intensity ratios are unrealistic since the direct signal can be depleted by two effects: (1) Anomalous attenuation due to incoherent scattering is normally greater near the ground; and (2) ray bending in the wind-shear layer near the ground can severely attenuate direct signals propagating against the wind. As observed in Fig. 6, the scattered signal from a vortex is often larger than the direct signal because of these effects.

Let us now examine the expected characteristics of a possible vortex tracking system. We assume a transmitter–receiver spacing of $D_1 = 300$ m and a centrally located B-747 vortex with a log core and a maximum scattering angle θ_m of 1.0 rad. The vortex can first be detected at a height of 75 m where the time delay of the scattered pulse is 120 msec according to Eq. (15). According to the analysis of Fig. 5(c), the horizontal-position error corresponding to a 2-msec error in time delay is about 8 m. The direct/scattered intensity ratio is 24 dB according to Eq. (18). When the vortex drifts down to its ground-effect height of 25 m, the scattering angle becomes 0.33 rad, the time delay 13 msec, the horizontal-position error 50 m, and the intensity ratio 14 dB. The normal atmospheric attenuation over 300 m is between 3 and 17 dB at 3 kHz, depending upon the humidity.[13]

This example illustrates the critical role played by the maximum scattering angle θ_m in this type of tracking system. In particular, if θ_m were only 0.3 rad, the vortex would be undetectable. In general, the upper altitude for tracking is set by θ_m and the lower altitude by the minimum acceptable error. Thus, the useful tracking area lies between the appropriate curves of Figs. 5(b) and 5(c). If θ_m is less than 0.5 rad, there is essentially no practical tracking area. The strong aircraft dependence of θ_m means that the capabilities of such a tracking system will vary drastically with aircraft type.

IV. DISCUSSION

Acoustic scattering techniques have recently become a popular means for the remote sensing of atmospheric turbulence.[14] These techniques are generally based on incoherent scattering which can be described by a perturbation calculation[14] where only a small fraction of the incident acoustic energy is scattered incoherently by the various Fourier components of the turbulence. The refractive scattering discussed here is produced by the organized motion of the vortex as a whole. The cross section σ for this scattering is much larger than that for scattering from random turbulence because of two effects. First, the entire incident beam is scattered rather than a small fraction. Second, the scattered energy is spread out in only one dimension (linear angle $d\sigma/d\theta$) rather than two (solid angle $d\sigma/d\Omega$). Another important distinction between the two types of scattering is the type of Doppler shift expected. Turbulence scattering gives a mean Doppler shift proportional to the average velocity of the wind which carries the turbulence along. Thus, the Doppler shift produced by incoherent scattering from turbulence imbeded in a vortex gives a measure of the velocities present in the vortex.[10,15] The ray-bending scattering from a stationary vortex has no Doppler shift because there is no change with time of the number of wavelengths along the propagation path. This scattering cannot measure the average wind velocity in the vortex because it is produced by the average wind. The only Doppler shifts to be expected are caused by changes in the vortex location.

The acoustic scattering from a real vortex will, of course, include both types of scattering. As a result, incoherent Doppler scattering may give an erroneous measurement of the wind velocity inside the vortex core. The Doppler shift is porportional to $\sin(\frac{1}{2}\theta_i)$ where θ_i is the incoherent scattering angle. Because of ray bending, the total scattering angle θ observed by a sensing system includes an additional component θ_c: $\theta = \theta_i + \theta_c$. If θ_c is an appreciable fraction of θ_i, one does not know $\frac{1}{2}\theta_i$ accurately and hence the derived vortex velocity may be in error. Obviously, large scattering angles θ alleviate this problem. Moreover, this difficulty would be encountered only for acoustic signals passing near the vortex core where θ_c is large.

APPENDIX

This appendix describes the procedure used for numerically evaluating Eqs. (1) and (6), and discusses the impact approximation which yields analytical expressions for $\theta(\rho)$ and $\tau(\rho)$.

The parameter s in the ray equation can be converted to the Cartesian coordinate x in Fig. 2 as long as the tangent vector $\mathbf{n}$ is not perpendicular to the x axis. The ray equations become

$$\alpha' = \gamma(r)/c\cos\alpha \ , \tag{A1a}$$

$$y' = \tan\alpha \ , \tag{A1b}$$

where α is the angle between $\mathbf{n}$ and the x axis, $r = (x^2 + y^2)^{1/2}$, and the prime denotes the x derivative. The vorticity $\gamma(r)$ is assumed to be negligible for $r > r_m$. The scattering angle $\theta(p)$ for the ray starting at impact parameter p is found by integrating Eqs. (A1) starting at $x = -(r_m^2 - p^2)^{1/2}$, $y = p$, and $\alpha = 0$ and continuing until $r > r_m$ where $\theta(p) = \alpha$. Since the ray path is symmetrical about the point where $\mathbf{n} \perp \mathbf{r}$ $(\alpha = \phi)$, one may terminate the integration there and obtain $\theta(p) = 2\alpha$. This procedure avoids the singularity $\tan\alpha = \infty$ which would arise for $\theta(p) \geq \frac{1}{2}\pi$. Equation (6) can be integrated along the ray to give

$$c\tau(p) = 2\left(\int_{-X}^{x^*} (\{1 - [v(r)/c]\,(\cos\alpha\cos\phi - \sin\alpha\sin\phi)\} \times \cos\alpha)^{-1}\,dx - X\right), \quad \text{(A2)}$$

where x^* is the point where $\alpha = \phi$ and the limit $X \to \infty$ is taken. Equations (A1) and (A2) were integrated by computer for the core models to obtain the results in Fig. 3. The program was checked by comparing θ_m with impact approximation values for weak vortices. The grid size was varied to verify that the results are accurate to better than several percent.

Equations (A1) and (A2) can be estimated for small scattering angles by means of the impact approximation which is well known in atomic scattering calculations. In this approximation Eqs. (A1a) and (A2) are integrated along the straight line path $y = p$ shown in Fig. 2. This approximation is valid when α is small enough that Eq. (A1b) can be ignored. The scattering angle becomes

$$c\theta(p) = 2\int_0^\infty \gamma(r)\,dx \quad \text{(A3)}$$

with $r = (x^2 + p^2)^{1/2}$ and the propagation-time change becomes

$$c^2\tau(p) = p\left(\int_0^\infty \frac{dx\,\Gamma(r)}{\pi r^2} - 2\theta(p)\right), \quad \text{(A4)}$$

where $v \ll c$ is assumed. The scattering angle $\theta(p)$ depends only upon $|p|$ and is in the direction of the vortex rotation. In general, $\gamma(r)$ will decrease monotonically with r so that θ has a maximum value θ_m for $p = 0$. The value of θ_m in Eq. (4) is thus given by setting $p = 0$ in Eq. (A3). One should note that for impact parameters well outside the vortex core ($p > r_m$) the impact approximation is exact to first order in v/c and Eq. (A4) reduces to the value of Eq. (7). The simple impact-approximation results for the core models are shown in Table I.

[1]T. M. Georges, "Acoustic Ray Paths Through A Model Vortex with a Viscous Core," J. Acoust. Soc. Am. **51**, 206–209 (1972).
[2]D. Burnham, R. Kodis, and T. Sullivan, "Observations of Acoustic Ray Deflection by Aircraft Wake Vortices," J. Acoust. Soc. Am. 52, 431–433 (1972).
[3]R. B. Lindsay, "Compressional Wave Front Propagation Through a Simple Vortex," J. Acoust. Soc. Am. 20, 89–94 (1948).
[4]R. F. Salant, "Acoustic Rays in Two-Dimensional Rotating Flows," J. Acoust. Soc. Am. 46, 1153–1157 (1969).
[5]L. D. Landau and E. M. Lifshitz, *Fluid Mechanics* (Pergamon, Oxford, 1959), p. 261.
[6]The extension of Eq. (1) to higher order in v/c can be carried out using the vector ray equation of P. Ugincius, "Acoustic-Ray Equations for a Moving, Inhomogeneous Medium," J. Acoust. Soc. Am. 37, 476–479 (1965). The second-order terms give the lowest-order deflection where $\gamma = 0$ and where found to bend the ray toward the core, as noted in the computer calculations of Georges.[1]
[7]J. R. Spreiter and A. H. Sacks, "The Rolling Up of the Trailing Vortex Sheet and Its Effect on the Downwash Behind Wings," J. Aeronaut. Sci. 18, 21–32, 72 (1951).
[8]E. R. Hoffman and P. N. Joubert, "Turbulent Line Vortices," J. Fluid Mech. 16, 395–411 (1963).
[9]B. W. McCormick, J. L. Tangler, and H. E. Scherrieb, "Structure of Trailing Vortices," J. Aircr. 5, 260–267 (1968).
[10]D. C. Burnham, T. E. Sullivan, and L. S. Wilk, "Measurement of Wake Vortex Strength by Means of Acoustic Back Scattering," J. Aircr. 13, 889–894 (1976).
[11]For a treatment which includes the effects of wind shear see D. C. Burnham, "Effect of Ground Wind Shear on Aircraft Trailing Vortices," AIAA J. 10, 1114–1115 (1972).
[12]D. C. Burnham and T. E. Sullivan, "Influence of Flaps and Engines on Aircraft Wake Vortices," J. Aircr. 11, 591–592 (1974).
[13]C. M. Harris, "Absorption of Sound in Air versus Humidity and Temperature," J. Acoust. Soc. Am. 40, 148–159 (1966).
[14]C. G. Little, "Acoustic Methods for the Remote Probing of the Lower Atmosphere," Proc. IEEE 57, 571–578 (1969).
[15]M. Balser, A. Nagy, and C. McNary, "Acoustic Back Scatter Radar System for Tracking Aircraft Trailing Vortices," J. Aircr. 11, 556–562 (1974).